Dependence of friction on roughness, velocity, and temperature

Yi Sang,[1] Martin Dubé,[2] and Martin Grant[1]
[1]*Physics Department, McGill University, Rutherford Building, 3600 rue University, Montréal, Québec, Canada H3A 2T8*
[2]*Centre Intégré en Pâtes et Papiers, Université du Québec a Trois-Rivières, Case Postale 500, Trois-Rivières, Québec, Canada G9A 5H7*

(Received 25 July 2007; published 27 March 2008)

We study the dependence of friction on surface roughness, sliding velocity, and temperature. Expanding on the classic treatment of Greenwood and Williamson, we show that the fractal nature of a surface has little influence on the real area of contact and the static friction coefficient. A simple scaling argument shows that the static friction exhibits a weak anomaly $\mu \sim A_0^{-\chi/4}$, where A_0 is the apparent area and χ is the roughness exponent of the surface. We then develop a method to calculate atomic-scale friction between a microscopic asperity, such as the tip of a friction force microscope (FFM) and a solid substrate. This method, based on the thermal activation of the FFM tip, allows a quantitative extraction of all the relevant microscopic parameters and reveals a universal scaling behavior of atomic friction on velocity and temperature. This method is extended to include a soft atomic substrate in order to simulate FFM scans more realistically. The tip is connected with the support of the cantilever by an ideal spring and the substrate is simulated with a ball-spring model. The tip and substrate are coupled with repulsive potentials. Simulations are done at different temperatures and scanning velocities on substrates with different elastic moduli. Stick-slip motion of the tip is observed, and the numerical results of the friction force and distribution of force maxima match the theoretical framework.

DOI: 10.1103/PhysRevE.77.036123 PACS number(s): 81.40.Pq, 46.55.+d, 07.79.−v, 83.50.Lh

I. INTRODUCTION

The empirical laws of friction between macroscopic surfaces were discovered long ago by Da Vinci, Amonton, and Coulomb. They found that friction is (i) independent of the apparent contact area, (ii) proportional to the normal load, and (iii) independent of the sliding velocity [1]. Although these laws are modified by plasticity [2], they remain essentially valid, and friction at the macroscopic level is now well understood, for both dry rough [3] and lubricated surfaces [4]. Nevertheless, the subject continues to be reconsidered, particularly in connection to developments in the field of nanotribology [5,6], to the new experimental possibilities of studying friction at the atomistic level opened by the atomic force microscope [7–13], and to the fractal structure inherent in several surfaces [5,14–24]. The contact problem between a plane and a rough surface is also of fundamental importance in several processes, such as printing on paper and board [25,26].

Macroscopic solids sliding against each other interact mainly through many atomic-scale asperities present on their surface. Although it is in essence a *macroscopic* phenomenon, the physics of friction thus extends over several length scales and depends crucially on the microscopic aspects of the problem. In this paper, we study separately two aspects, microscopic and macroscopic, of friction.

The macroscopic collective effect of all the asperities is measured through the friction coefficient μ, defined as the ratio between the tangential force F needed to slide surfaces at velocity v and the normal load F_n applied on them: $\mu = F/F_n$. From Amonton's law, the friction coefficient is independent of the apparent contact area of the sliding solids. This holds for nominally rough surfaces [3] but not necessarily for *self-affine* surfaces, where the roughness depends on the length scale of observation. Since many real surfaces show self-affine behavior over some length scales [23,24], it is important to know if Amonton's law is modified in this case. Several very detailed studies on this topic have shown that the fractal character of the surface has very little effect, or none at all, on the real area of contact. We show that the earlier treatment of Greenwood and Williamson [3] can be used even in the case of self-affine surfaces and calculate the contact area between rough self-affine surfaces. We show how both the area of real contact, and the friction coefficient between them, depend on the roughness exponent χ of the surfaces. We find that the real area of contact A_r between a plane and a self-affine fractal surface scales as $F_n \sim A_r^{\beta}$ where $\beta = (4+3\chi)/(4+2\chi)$. For a self-affine surface, $0 < \chi < 1$, leading to $1 < \beta < 7/6$, in good agreement with recent numerical results of Batrouni *et al.* [17], and in line with other recent work [16,18–21] predicting also an almost linear relationship between the normal force and the real contact area of the surface. We also find that the friction coefficient has a weak anomalous dependence on the apparent contact area A_0 through the roughening exponent, namely, $\mu \propto A_0^{-\chi/4}$, which in principle is measurable experimentally.

The study of friction at the microscopic level of the asperity has gained importance over the years, particularly with respect to the field of nanotechnology. An understanding of friction at this level is also necessary to make the link to the global behavior of the asperities. Friction at the single-asperity level is ideally explored by the friction force microscope (FFM), whose tip consists of only a few atoms [7–9,27,28]. At low scanning velocities, FFM experiments found that the tip can exhibit stick-slip behavior commensurate with the periodicity of the substrate's underlying lattice. As the FFM measures friction force F under a constant load, this gives the effective microscopic friction coefficient μ_{micro}

as $\mu_{\text{micro}} \propto F$ under those conditions. That is, the FFM essentially provides experimental access to the friction of a single asperity, under weak loading, linear response conditions.

The situation can be studied using a simplified Tomlinson model [29–32], and a detailed analysis of thermal effects on the stick-slip behavior, treated as a dynamic critical phenomenon [33–38], shows that the friction force F decreases from its optimal value of F_c at $T=0$, with a correction of the form [6,39,40]

$$F - F_c \propto -T^{2/3} \ln^{2/3}\left(B\frac{T}{v}\right), \tag{1}$$

where F is the friction force, T is temperature, and v is the scanning velocity. As noted above, the microscopic friction coefficient $\mu_{\text{micro}} \propto F$. The nonuniversal constant B depends on the exact details of the setup [39]. We have shown before that this result compares well to numerical simulations when the FFM tip can be described by a simple Langevin equation with a *static* periodic potential coming from the substrate. We show in the present paper that this result also holds when elasticity of the substrate, modeled as a ball-spring system, is included, provided the substrate is sufficiently rigid.

The rest of the paper is organized as follows. Section II shows the friction coefficient's dependence on surface roughness. In Sec. III theoretical and numerical calculations of the friction force between a FFM and a substrate are presented. Conclusions are summarized in Sec. IV.

II. CONTACT AND FRICTION BETWEEN ROUGH SURFACES

Several experimental studies (see, e.g., Chap. 4 of Ref. [5]. or Refs. [23,24]) have shown that surfaces often present a self-affine character over several length scales. Hence, the contact mechanics between rough surfaces has been the subject of several recent studies [15–22]. Knowledge of the contact area between rough surfaces is the first step in the study of friction on rough surfaces. However, it is often argued that a fractal surface possesses asperities on all length scales so that the usual treatments, based on the contact mechanics of individual asperities with a surface [3], are not valid. In contrast, here we consider the realistic case of a standard rough surface. Such a surface is assuredly self-affine on large length scales, but on small length scales such behavior is modified by the presence of a small-length-scale ultraviolet cutoff.

Consider a rough surface in contact with a flat plane. The rough surface, of height $h(\mathbf{x})$, is assumed to be a self-affine fractal in the range $a<x<L$. The length a is a *physical* microscopic cutoff length, typically of the order of a few nanometers, at which the fractal behavior breaks down. The length scale $L \sim A_0^{1/2}$ is the lateral size of observation, with A_0 is the apparent area of the surface. It is also possible that the self-affine character is present only up to an upper length scale ξ, of the order of a few micrometers. The surface is characterized by a power spectrum in d dimensions

TABLE I. Numerical value of the length l_δ for various values of the total width w for an apparent area $A_a = 10 \times 10\ \mu\text{m}^2$, a roughness exponent $\chi = 1/2$, and molecular cutoff length $a = 0.5$ nm

w (nm)	l_δ (nm)	κ (10^9 m^{-1})	$\mathcal{A}$
5	0.0025	0.14	400 μm^2
10	0.01	0.28	1.56 μm^2
50	0.25	1.41	4 nm^2

$$\langle |h_k|^2 \rangle = \Delta^2 k^{-d-2\chi}, \tag{2}$$

where h_k is the Fourier transform of the surface, χ is the roughness exponent, and $\langle \cdots \rangle$ represents an average over the statistical distribution of the interface [41]. In real space, the self-affine structure is determined by the correlation function

$$\langle [h(\mathbf{r}+\mathbf{l}) - h(\mathbf{r})] \rangle^{1/2} \sim l^\chi. \tag{3}$$

For $\chi < 1$, the amplitude of the power spectrum can be expressed in terms of a length $\Delta = (l_\delta)^{1-\chi}$ [42]. The total width of the interface,

$$w = \Delta L^\chi \sim l_\delta^{1-\chi} A_0^{\chi/2}, \tag{4}$$

depends on the apparent area of observation. The roughness exponent must satisfy $\chi < 1$ for the surface to be well defined. Its value depends on the universality class of the phenomenon [41]. For example, in the case of simple linear roughening, $\chi = (3-d)/2$ in d $(1<d<3)$ dimensions and logarithmic roughness in three dimensions. For several other common surfaces, the roughness exponent may be quite large, $0.5 < \chi < 0.9$, and w typically is of the order of a few tens of nanometers for a lateral length scale of the order of 1 μm [5]. In most cases, however, the length $l_\delta \ll a$, as shown in Table I.

A possible starting point to obtain the contact area between the rough surface and the plane is the general formula [43]

$$\mathbf{u}(\mathbf{r}) = \int d\mathbf{r}'\ G_{ik}(\mathbf{r}-\mathbf{r}')\sigma_k(\mathbf{r}'), \tag{5}$$

where $\mathbf{u}$ are the displacements induced by the normal stress σ_k over the surface $\mathbf{r} = (x, y)$ and the Green's function $G(r) \sim 1/r$ asymptotically. An early scaling analysis of Eq. (5), using a self-affine fractal surface on all length scales, predicted that the normal force F_n and the area of real contact would be related as $F_n \sim A_r^{(1+\chi)/2}$ [14]. However, in marked contrast, a numerical solution of Eq. (5) by Batrouni *et al.* [17] found $F_n \sim A_r^{1.1}$ for both $\chi = 0.6$ and $\chi = 0.9$. A detailed analysis by Persson [15], starting essentially from Eq. (5), but for a self-affine surface only over a limited range, shows $F_n \sim A_r$ unless the load is so large that the area of real contact becomes similar to the nominal area, probably far above the plastic threshold. The very weak dependence of the area of real contact on the roughness exponent is further confirmed by the multiscale analysis of Hyun *et al.* [18,19] and modified Green's function methods [20,21]. These results point to the fact that the self-affine nature of the surface has only

little influence on the contact mechanics, contrary to natural expectations.

This small effect of the self-affine surface is easily understood by realizing that in contact mechanics the important quantity is not necessarily the height itself or the height-height correlations [19], but rather the *mass density*, which is essentially

$$\rho(z) = \rho_0 \langle \theta(z - h(\mathbf{r})) \rangle, \tag{6}$$

where ρ_0 is the bulk density, and $\theta(u>0)=1$ and $\theta(u<0)=0$. This mass density should be used, rather than the asperity height distribution usually considered in traditional treatments of the problem.

For a self-affine surface with roughness exponent $\chi<1$, the ratio $w(L)/L \to 0$ as $L \to 0$, meaning that the surface is asymptotically flat and that there cannot be any long-range correlations in the mass density (see also Ref. [22]). For an interface with Gaussian fluctuations, it is straightforward to show that $\rho(z)=\mathrm{erfc}(z/w(A_0)$ [44], where $w(A_0) \sim A_0^{\chi/2}$ is the surface standard deviation of heights. In a general case, the mass density, or, equivalently, the height distribution, is well approximated asymptotically by the exponential form

$$\rho(z) \simeq \rho_0 e^{-z/w}. \tag{7}$$

The important point is of course that it has a finite range in the direction perpendicular to the surface.

The average curvature of the rough interface is obtained from $\kappa=\langle(\nabla^2 h)^2\rangle^{1/2}$, written explicitly as [44]

$$\kappa^2 = \int_{L^{-1}}^{a^{-1}} dk\, k^{3+d} \langle |h_k|^2 \rangle = a^{-2} \left(\frac{l_\delta}{a} \right)^{2(1-\chi)}. \tag{8}$$

Even though it depends on the short-distance cutoff, this is also a well-defined quantity. For typical surfaces, $10^{-2} < \kappa a \leq O(1)$ and we can therefore think of the surface as a set of $N_0 \sim A_0/\kappa^2$ asperities with radius of curvature κ^{-1} ranging from a few nanometers to a fraction of a micrometer.

It is then straightforward to use previous theories of contact mechanics due to Greenwood and Williamson [3] for rough surfaces. In this theory, the rough surface is composed of many distinct asperities. The contact of each asperity with the flat surface is treated within Hertz theory [45,46], which states that the contact area between the surface and the asperity is proportional to the ratio of the normal displacement to the curvature $(z-u)/\kappa$, where u is the separation between the two surfaces, z is the height of the asperity, and κ the curvature of the asperity. The normal force is proportional to $E_* \kappa^{-1/2} (z-u)^{3/2}$, where E_* is the effective elastic modulus of the surfaces [47]. With an exponent distribution of density, all the standard results of the theory follow. If the total number of asperities on the surface is N_0, the number of asperities in contact is

$$N = N_0 e^{-u/w}, \tag{9}$$

and the total real contact area A_r and normal load F_n of all the asperities in contact are

$$A_r = N_0 \kappa^{-1} w e^{-u/w} = (w/\kappa) N, \tag{10}$$

$$F_n = N_0 E_* (w^3/\kappa)^{1/2} e^{-u/w} = E_* (w\kappa)^{1/2} A_r. \tag{11}$$

Since the curvature is a well-defined quantity, the number of asperities is related to the apparent area of contact via $N_0 \sim A_0 \kappa^2$, and the relation between the real area of contact and the normal force can be established for different values of u. In the limit $u \ll w$, the exponential term can be neglected and $N \approx N_0$. Using Eq. (4) to express the width w in term of the apparent area A_0, the apparent and real areas of contact are related through Eq. (10) as

$$A_0 = \mathcal{A} \left(\frac{A_r}{\mathcal{A}} \right)^{2/2+\chi}, \tag{12}$$

where the area

$$\mathcal{A} = l_\delta^2 \left(\frac{a}{l_\delta} \right)^{2(2/\chi-1)} \tag{13}$$

ranges between a few nm^2 and several $\mu\mathrm{m}^2$ (see Table I). In this limit, the relation between the normal force and the real area of contact is

$$F_n = E_* \mathcal{A} \left(\frac{A_r}{\mathcal{A}} \right)^{\beta}, \tag{14}$$

where the exponent β

$$\beta = \frac{4+3\chi}{4+2\chi}, \tag{15}$$

For $0<\chi<1$, the exponent $1<\beta<7/6$.

The width is itself related to the real contact area, so the range of validity of this power-law regime is obtained self-consistently as

$$\frac{u}{w} = u\kappa \left(\frac{\mathcal{A}}{A_r} \right)^{\chi/2+\chi} \ll 1, \tag{16}$$

meaning that large apparent and real surfaces of contact are necessary. The parametric plot of Fig. 1 shows that the power-law relationship between the real area and the force is actually valid over a wide range of parameters. Deviations from Eq. (14) occur only when $u\kappa(a_0/A_r)^{2/(2+\chi)} \gg 1$, in which case we obtain $F_n \sim A_r^{\beta/2}$.

The weak dependence of β on χ, and the range of values for β, are in good agreement with numerical results of Batrouni *et al.* [17]. Those authors found that $F_n \simeq A_r^{1.1}$—that is, $\beta \approx 1.1$, for both $\chi=0.6$ and $\chi=0.9$. It is, however, not in agreement with the linear behavior obtained by Persson [16] as well as by Hyun *et al.* [18,19] and Campana [20,21]. This disagreement may come from the fact that the transverse displacement of the surface must be carefully taken into account during the contact process. Large system sizes must also be considered in order to deal with such small exponents. Nevertheless, our result, which is obtained from the finite range of the asperity height distribution, again points to the weak effect of a fractal surface on the real area of contact.

A simple argument may then be used to estimate the static coefficient of friction. Assuming that most of the asperities are in a state of incipient plastic flow, and that the previous

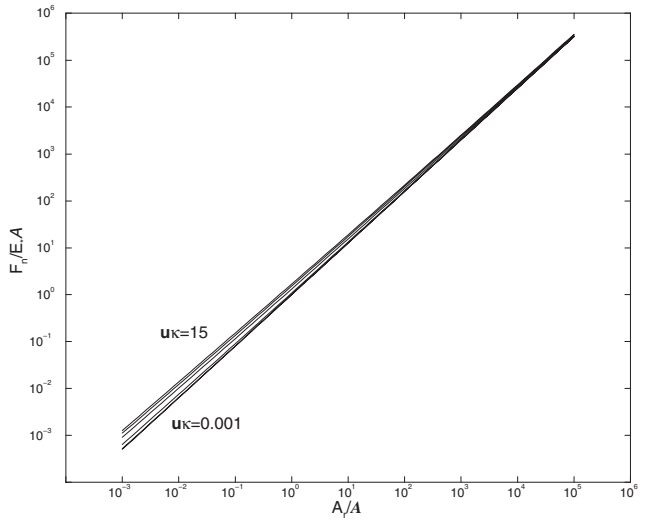

FIG. 1. Relation between the normal force and the real area of contact for a surface characterized by $\chi=0.5$ and values of the dimensionless parameters $u\kappa=10^{-3}$ (lowest curve) 10^{-2}, 1, 5, 10, and 15 (highest curve). The slope of the lines corresponds to the exponent β [Eq. (15)], with only very weak deviations at small loads.

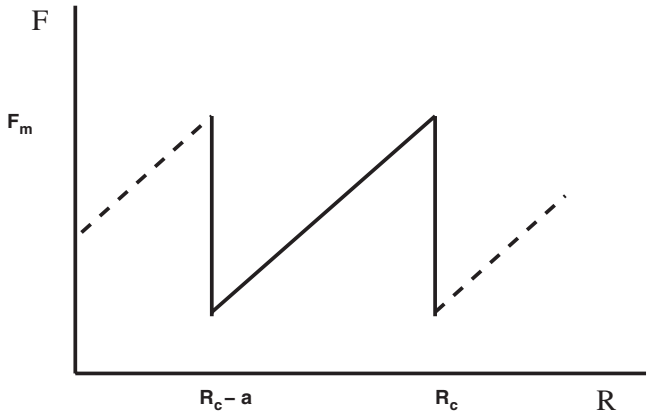

FIG. 2. Idealized friction force measured during a stick-slip event at zero temperature. As the support moves away, the force increases linearly until a position R_c (to which corresponds a maximal force F_m). At this point, the energy barrier opposing the motion of the tip vanishes, the tip is released, and the force decreases suddenly. At nonzero temperature, thermal activation can cause transitions for positions $R \leq R_c$. The position at which this transition occurs as well as the maximal force registered between the events are then stochastic quantities whose distribution is related to Eq. (28) of the text.

result, based on linear elasticity is not drastically modified, the lateral force necessary to displace the asperities is $F \sim \sigma_c A_r$ where the yield stress is σ_c [4]. Then, using Eqs. (9) and (10), we find that the friction coefficient $\mu \equiv F/F_n$ depends on the width of the interface: $\mu \propto w^{-1/2}$. Immediately, then, from the dependence of the width on the apparent area of contact in Eq. (3), we obtain the anomalous dependence of the friction coefficient on the apparent area of contact,

$$\mu(A_0) \propto A_0^{-\chi/4}. \tag{17}$$

This transport-coefficient anomaly is measurable experimentally, as well as numerically, provided that the load dependence on the area of contact is also taken into account [20]. In any case, this is a very weak dependence; as mentioned above, on general grounds $\chi < 1$.

At fairly large loads, plasticity leads to an increase in the contact area over time. Heslot *et al.* [2] have shown that for large load values (~ 1 N) but very small pulling velocities ($v < 1$ μm/s), the friction coefficient $\mu = \mu(v)$, together with stick-slip motion caused by the plastic relaxation of the contact. On the other hand, at very small loads, the stick-slip phenomenon, caused solely by interatomic forces between the asperities and the surface periodic potential, occurs [8]. We now concentrate on this case.

III. STICK-SLIP BEHAVIOR AND THERMAL ACTIVATION

A friction force microscope provides direct access at the atomic level to friction. As such, it essentially probes the friction of a single asperity, under weak loading, linear response conditions. In this section, we present the general stick-slip phenomenon in atomic friction and introduce a simple one-dimensional model to calculate atomic-scale friction. For the measurement probe, we refer explicitly to the FFM, modeled as a tip coupled elastically to a moving cantilever [7–9].

In a typical experimental situation, the FFM is dragged in contact mode across a surface at constant velocity, and the friction force F needed for this continuous displacement is recorded as a function of R, the displacement of the cantilever. The occurrence of stick-slip behavior is then seen as a series of triangular force jumps (Fig. 2) with the periodicity of the substrate lattice spacing. As noted above, this force is proportional to the microscopic friction coefficient μ_{micro}.

This behavior can be understood from an analysis of the energetics of the tip. If the tip of a FFM, put close to a substrate, its global energy is the sum of two terms: the lattice surface potential and the elastic coupling between the tip and the cantilever. A typical superimposition of these two potentials is shown in Fig. 3. Most of the time, the tip remains static at potential minima [see Fig. 3(a)]. As the cantilever is displaced, the elastic force F increases while the potential barrier decreases [see Fig. 3(b)]. At low temperatures, the tip barely moves until the potential barrier vanishes, at which point it jumps to the next potential minimum, thus causing a sudden decrease in the friction force [see Fig. 3(c)]. At nonzero temperature, thermal fluctuations make it possible for a jump to occur *before the barrier vanishes*, when it becomes comparable to $k_B T$.

A. Analysis

For commensurate surfaces, we treat the tip as a point particle, with coordinate $\mathbf{r} = (x,z)$ [48], subject to an effective substrate surface potential $U(\mathbf{r})$, which possesses the periodicity of the substrate, $U(x+a,z) = U(x,z)$, where a is the lattice constant of the surface. Sinusoidal functions are com-

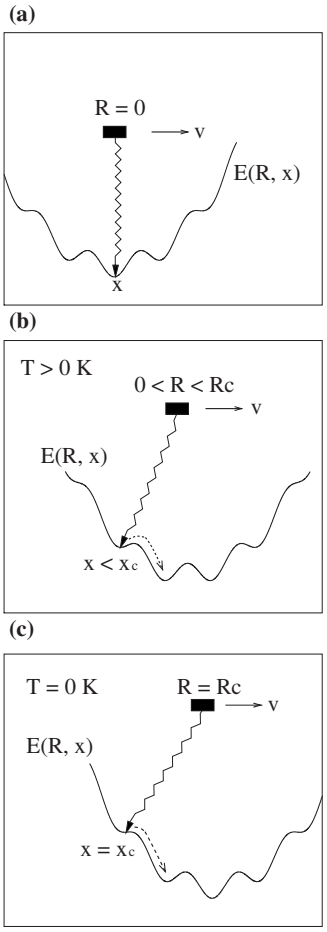

FIG. 3. Schematic plots of the potential function $E(R,x)$ vs x, the position of the tip, for different positions R of the support.

monly used to model this part of the surface potential [11,30,31,39]. In the special case of a FFM operating under constant load, the normal force is fixed and the z coordinate drops out of the problem. The second potential is the elastic coupling between the tip and the cantilever, $K(R,x)$, where R is the coordinate of the cantilever support [30,31,39].

The global energy of the tip is thus [see Fig. 3(a)]

$$E(R,x) = U(x) + K(R,x). \tag{18}$$

In this section, we keep $U(\mathbf{r})$ and $K(R,x)$ as general functions. Specific forms appropriate to the case of a FFM on a surface will be given in the next section.

For a given support position R, the equilibrium position of the tip, denoted $x_{\mathrm{eq}}(R)$, is obtained by

$$\frac{\partial E[R,x_{\mathrm{eq}}(R)]}{\partial x} = 0, \tag{19}$$

and the friction force measured experimentally corresponds to

$$F = \left.\frac{\partial K(R,x)}{\partial x}\right|_{x_{\mathrm{eq}}} \cong \tilde{k}R. \tag{20}$$

The second part of Eq. (20) is a linear approximation to the friction force. It introduces the effective elastic constant $\tilde{k}$ which accounts for the effect of the potential $U(x)$ on the elastic force of the FFM [39]. The effective constant $\tilde{k}$ corresponds to the slope of the friction force in the sticking part of a typical sawtooth figure (see Fig. 2).

The critical point at which the energy barrier vanishes corresponds to an inflection point of the global potential. For this position of the support R_c (to which corresponds an equilibrium position of the tip x_c), both the first and second derivatives of $E(R,x)$ at x_c are zero,

$$\frac{\partial E(R_c,x_c)}{\partial x} = 0 \tag{21}$$

and

$$\frac{\partial^2 E(R_c,x_c)}{\partial x^2} = 0. \tag{22}$$

At nonzero temperature, the tip is thermally activated over the energy barrier to the next potential minimum before R reaches R_c. Since we expect this actual jump to take place on time scales much faster than the typical time spent in a potential well, we can describe this transition by the Kramers rate [49] in the potential corresponding to the *instantaneous* position R,

$$\tau^{-1}(R) = \frac{\Omega^2}{2\pi\gamma} e^{-\Delta E/k_B T}, \tag{23}$$

where Ω and ΔE correspond, respectively, to the effective oscillation frequency and barrier height, and γ is the dissipation coefficient. Due to this exponential behavior, the greatest probability for a transition to occur is in the region $\Delta E \ll k_B T$. In this case, Eq. (A6) shows that, to lowest order in the bias $f \equiv 1-(R/R_c) \ll 1$, the energy barrier and oscillation frequency of a general potential of the form $E(R,x)$ are

$$\Delta E = E_{\mathrm{eff}} f^{3/2} \tag{24}$$

and

$$\Omega = \Omega_{\mathrm{eff}} f^{1/4}, \tag{25}$$

where the constants E_{eff} and Ω_{eff}, given in Eqs. (A7) and (A11), are expressed in terms of derivatives of $E(R,x)$ at *the critical position*. The effective energy barrier is in general a complex interplay between the substrate elastic energy, the structure of the tip, and the normal load applied to the tip and can be measured experimentally [9–11].

For a support moving at constant velocity, $R(t)=vt$. The probability that a transition has not taken place at time t is [35,37,39]

$$W(R(t)) = \exp - \int_{t_0}^{t} \tau^{-1}[R(t')]dt'. \tag{26}$$

Changing the variable from t' to R, the distribution of the support's position at which a transition occurs, i.e., R_m, is then obtained as

$$P(R_m) = -\frac{dW(R)}{dR} \tag{27}$$

$$= \frac{3}{2} X f^{*1/2} \exp(-f^{*3/2} - X e^{-f^{*3/2}}), \tag{28}$$

where $f^* = (E_{\text{eff}}/k_B T)^{2/3} f$ and

$$X = \frac{2}{3} \frac{\Omega_{\text{eff}}^2}{2\pi\gamma} \frac{R_c}{v} \frac{k_B T}{E_{\text{eff}}}. \tag{29}$$

From the distribution of the transition positions $P(R_m)$, we calculate the average transition position [37]

$$\langle R_m \rangle = R_c - R_c \left(\frac{k_B T}{E_{\text{eff}}} \right)^{2/3} g(X), \tag{30}$$

where the function $g(X) \sim \ln^{2/3} X + O(1/\ln X)$ in the limit $X \gg 1$ [35,37] and $g(X) \sim X + O(X^2)$ in the limit $X \ll 1$.

With the linear approximation Eq. (20) between F and R, it is straightforward to calculate the average lateral force as the integral of the instantaneous force over a cycle of the stick-slip motion, which yields [51]

$$F = F_c - \Delta F(T)[\ln X(v,T)]^{2/3}, \tag{31}$$

where the constants

$$F_c = \tilde{k} \left(R_c - \frac{a}{2} \right), \tag{32}$$

$$\Delta F = \tilde{k} R_c \left(\frac{k_B T}{E_{\text{eff}}} \right)^{2/3}, \tag{33}$$

and $X(v,T)$ is presented in Eq. (29). As noted above, this is proportional to μ_{micro}, and is, in essence, the friction of a single asperity—under weak loading and linear response conditions. The incoherent average of many such asperities gives the friction coefficient, albeit under those quite restricted conditions.

As the velocity of the support is increased, the tip spends less and less time in the minima of the potential wells. When a velocity v^*, defined by $X(v^*,T)$, is reached, thermal fluctuations do not act on a time scale sufficiently fast to activate the tip and the friction force reaches the static zero-temperature limit as $F_c - F \sim T^{5/3}/v$. Once $F = F_c$, the friction force remains at this plateau, as already seen experimentally [9]. The behavior continues until viscous friction $F_v = M\gamma v$ dominates. Comparing the viscous and potential forces yields the velocity v_c at which this occurs:

$$v_c = \frac{\partial U(x_c)/\partial x}{M\gamma}. \tag{34}$$

Note that the ratio v^*/v_c is independent of γ.

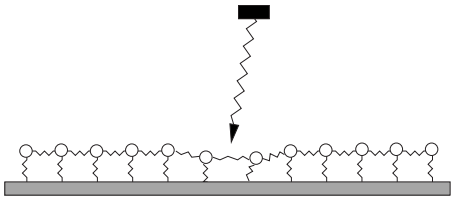

FIG. 4. Schematic diagram of the numerical model. FFM tip is modeled with a tip coupled elastically to a support and the substrate is modeled with a ball-spring model.

The maximal force F_m between tip and cantilever before a transition occurs decreases from its optimal value at $T=0$ and becomes a stochastic quantity [39]. Assuming $F_m \sim \tilde{k} R_m$, its distribution is obtained directly from Eq. (28). We show in Sec. III B that there is a good agreement between Eqs. (31) and (28) and the numerical simulations. The exponent 2/3 in Eq. (31) comes from the nonlinear characteristic of Eqs. (24) and (25). As we show in the Appendix, those nonlinear characteristics are universal for problems with transition close to the critical position, and do not depend on any particular form of the global energy.

B. Numerical model

To test the method developed in the last section, we set up an atomistic model to simulate the operation of a FFM. A schematic graph of the model is shown in Fig. 4. The tip, with coordinate $\mathbf{r} = (x,z)$, and its coupling to the cantilever are modeled by a single atom attached to a moving support. The support of the cantilever has coordinates $\mathbf{R} = (R,Z)$. For operation under constant load, the separation between the support and the tip in the normal direction, $Z - z$, remains constant at all times. The support moves horizontally at constant velocity v, $R = vt$. The support and the tip are connected by a spring with spring constant k, and the elastic energy between the tip and the support is

$$K(R,x) = \frac{1}{2} k (R - x)^2 \tag{35}$$

We set the numerical value $k = 0.93$ N/m, typical of experimental setups [8,9,39].

The substrate is modeled using a ball-spring model [50]. Twenty atoms with coordinates $\mathbf{r}_i = (x_i, z_i)$ and equilibrium position $\mathbf{r}_{i,0} = (x_{i,0}, z_0)$ are connected with springs and satisfy periodic boundary conditions. The original positions of these atoms are $x_{i,0}$ and $z_{i,0}$ and they are connected to a rigid second layer. The atoms are held in their original positions with harmonic potentials described by spring constants k_{xz} and k_{zz}, while the spring constant of the lateral springs between the atoms is k_{xx}. The elastic energy of the substrate atoms is

$$V_{\text{sub}}(\{\mathbf{r}_i\}) = \sum_i \frac{1}{2} k_{xz} (x_i - x_{i,0})^2 + \sum_i \frac{1}{2} k_{zz} (z_i - z_{i,0})^2 + \sum_i \frac{1}{2} k_{xx} (x_{i+1} - x_i - a)^2, \tag{36}$$

where the lattice constant $a = 0.4$ nm. Different values of k_{xx},

k_{xz}, and k_{zz} correspond to substrates with different elastic moduli. In the x direction (the scan direction) the shear modulus $G=k_{xz}/a$, while the compressibility is described by the modulus $B_x=(2k_{xx}+k_{xz})$. The bulk compressibility in the z direction $B_z=k_{zz}/a$. It is not our intention to describe a surface in all its details, but rather to consider the effect of the elasticity of a substrate on the theoretical prediction of Eq. (1). Equation (36) then defines the simplest model that allows us to interpolate between a completely rigid and a very soft substrate.

The interaction potential between the tip and substrate atoms is modeled using an exponential repulsive potential,

$$V_{\text{int}}(\mathbf{r},\{\mathbf{r}_i\}) = \sum_i V_0(e^{r_0/|\mathbf{r}-\mathbf{r}_i|} - 1), \tag{37}$$

where $|\mathbf{r}-\mathbf{r}_i|=\sqrt{(x-x_i)^2+(z-z_i)^2}$ is the displacement between the tip and the substrate atom i. We set $V_0=0.049$ eV and $r_0=2a$.

A common alternative for the interaction potential is the Lennard-Jones potential [50]. Since FFMs are typically operated in contact mode, the tip and substrate separation is small and the force between them is repulsive. Long-range van der Waals attractive forces are trivial in this situation. The choice between the exponential repulsive potential and Lennard-Jones potential will not alter the final results. Another potential in the system is the potential due to the load, which is $F_n(z-z_0)$ [50]. The total potential energy of the whole system is then

$$E = K(R,x) + V(\mathbf{r},\{\mathbf{r}_i\}) + F_n(z-z_0) + V_{\text{sub}}(\mathbf{r},\{\mathbf{r}_i\}). \tag{38}$$

The operation of the FFM under constant load uses a feedback loop to keep the separation between the tip and cantilever constant. We thus allow the tip to follow the surface smoothly in the vertical direction by adjusting the coordinate z such that the normal force

$$F_n = -\frac{\partial V_{\text{sub}}}{\partial z} \tag{39}$$

remains fixed at all times.

The local deformations of the substrate spread at the speed of sound ($\sim 10^4$ m/sec), and so the typical time scales associated with the substrate $\sim 10^{-13}$ sec. In contrast, the tip of the mass is several orders of magnitude greater that the mass of the atoms in the substrate, with much larger time scales [$\sim\Omega^{-1}$; see Eq. (25)]. Typical scans are over several lattice spacings, at velocities ranging from a few nm/sec to the range of μm/sec, and a full molecular dynamics simulation, extending over a time $\sim 10^{-3}$ sec that would encompass both the time scales of the substrate and tip is thus unrealistic. However, on the time scales relevant to the tip motion, the energy transferred from the tip to the substrate is dissipated almost instantly, and the fast motion of the substrate can be incorporated phenomenologically into a Langevin equation for the lateral motion of the tip alone [52,53]:

TABLE II. Values of load and elastic constants chosen for the simulations. The basic unit of the elastic constant is $k=0.93$ N/m, related to the elasticity of the FFM [Eq. (35)]. The shear strain ϵ corresponds to the maximal displacement of the substrate atoms under the motion of the tip and characterizes the softness of the substrate.

ϵ	F_N (nN)	$k_{xx}(kxx/k)$	k_{xz} (k_{xz}/k)	k_{zz} (k_{zz}/k)
0.01	2.2	120	160	400
0.05	1.6	12	16	40
0.1	1.6	4	4	12

$$M\frac{d^2x}{dt^2} + M\gamma\frac{dx}{dt} - k(R-x) - f_x = \xi(t), \tag{40}$$

where M is the effective mass of the tip (chosen to be $M=8.7\times 10^{-12}$ kg). The fast degrees of freedom of the substrate are present through the dissipation coefficient γ ($\gamma=8.9\times 10^5$ sec^{-1}) and the random noise ξ, satisfying the fluctuation-dissipation relation $\langle\xi(t)\xi(t')\rangle=2M\gamma k_BT\delta(t-t')$, where the angular brackets denote an average, and k_B is Boltzmann's constant. The total lateral force applied on the tip by the substrate is

$$f_x = -\frac{\partial V_{\text{int}}}{\partial x} = \sum_i V_0 e^{r_0/r_i}\frac{r_0}{r_i^2}\frac{x-x_i}{r_i}. \tag{41}$$

The slow motion of the substrate is obtained by letting the substrate totally relax to equilibrium at each time step, i.e., for a given position $\mathbf{r}$ of the tip, the position of each atom of the substrate $\mathbf{r}_i$ is set by

$$\frac{\partial V_{\text{int}}}{\partial x_i} + \frac{\partial K_{\text{sub}}}{\partial x_i} = 0,$$

$$\frac{\partial V_{\text{int}}}{\partial z_i} + \frac{\partial K_{\text{sub}}}{\partial z_i} = 0. \tag{42}$$

The effect of the thermal fluctuations of substrate atoms around their equilibrium positions was tested and we found that its impact is negligible [54].

C. Comparison of analysis and numerical results

We study the influence of the elasticity of the substrate, with comparison to the theoretical model of Sec. III A, by adjusting the elastic constants of the substrate k_{xx}, k_{xz}, and k_{zz} to produce different values of shear strain $\epsilon=0.01$, 0.05, and 0.1. This last value is just below typical criteria for surface melting [55].

Equation (40) is simulated using Ermak's algorithm [52]. The parameters used in the calculations are shown in Table II. For each temperature and velocity, the scanning distance is 50 lattice spacings and time steps are between $0.01/\gamma$ and $0.07/\gamma$. The simulations are done at several temperatures and velocities for each substrate. For the hard substrate [$\epsilon=0.01$; see Fig. 5(b)], we use four different temperatures, 133, 213, 293, and 373 K, with scanning velocities 5 nm/sec$\leq v$

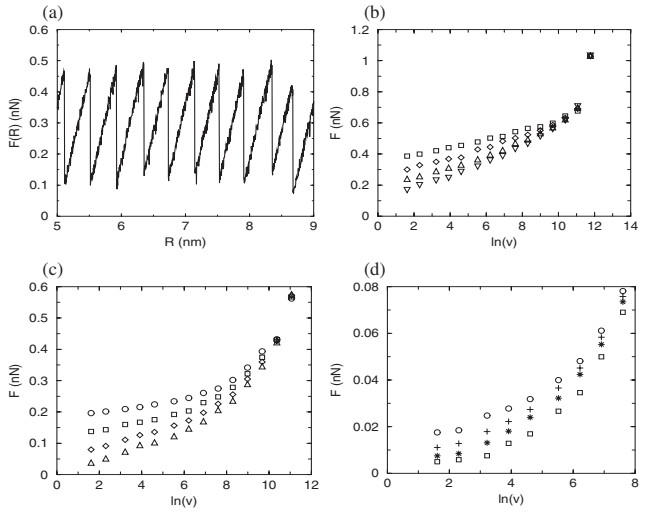

FIG. 5. (a) Typical stick-slip behavior of the instantaneous friction force as the support is moved at velocity $v=25$ nm/sec for a temperature $T=293$ K on hard substrate ($\epsilon=0.01$). (b) shows average friction force for different velocities at different temperatures for the same substrate. Squares, diamonds, up triangles, and down triangles correspond, respectively, to temperatures $T=133$, 213, 293, and 373 K. (c) shows average friction force for different velocities at different temperatures for mid-soft substrate ($\epsilon=0.05$). Circles, squares, diamonds, and up triangles correspond, respectively, to temperatures $T=53$, 133, 213, and 293 K. (d) shows average friction force for different velocities at different temperatures for soft substrate ($\epsilon=0.1$). Circles, pluses, stars, and squares correspond, respectively, to temperatures $T=53$, 73, 93, and 133 K. The units of velocity v are nm/sec.

≤ 256 μm/sec. For the softer substrates, the simulations must be performed at lower temperatures. For the $\epsilon=0.05$ substrate [Fig. 5(c)], we use 53, 133, 213, and 293 K with scanning velocities 5 nm/sec $\leq v \leq 64$ μm/sec. Finally, for the softest substrate [$\epsilon=0.1$; Fig. 5(d)], we use 53, 73, 93, and 133 K, with 5 nm/sec $\leq v \leq \mu$m/sec. Smaller loads are used for the softer substrate, so as to obtain equivalent indentation of the surface.

The general results show an increase of the friction force with velocity and a decrease with temperature. At high velocities, stick-slip behavior disappears and linear friction $F \sim M\gamma v$ starts to dominate. This corresponds to the sharp increase in Figs. 5(b)–5(d).

In order to apply the method developed in Sec. III A to the numerical model of Sec. III B, we need to know the effective surface potential $U(x)$, introduced in Eq. (18). This is not trivial since the interaction potential V_{int} is a function of both x and z, with z constantly changing to maintain a constant load. However, the collective effect of the substrate and load is included in Eq. (40), and we can associate

$$\frac{\partial U(x)}{\partial x} \equiv -f_x(x,z(x),\{\mathbf{r}_i(x)\}), \tag{43}$$

where the transverse position of the tip and the position of the substrate are obtained from Eqs. (39) and (42). This quantity can be obtained numerically from a simulation of

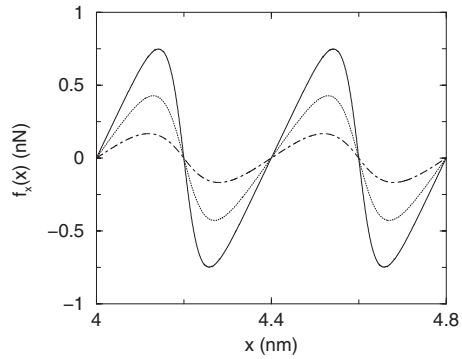

FIG. 6. Resistance force applied on the tip by the substrate atoms for three different substrates. Solid, dashed, and dot-dashed lines correspond, respectively, to hard ($\epsilon=0.01$), mid-soft ($\epsilon=0.05$), and soft ($\epsilon=0.1$) substrates.

Eq. (40) at $T=0$ (see Fig. 6). Once f_x is known, higher-order derivatives of $U(x)$ are obtained by numerical differentiation. The critical position x_c is found from Eq. (21),

$$\frac{\partial^2 E(R_c,x_c)}{\partial x^2} = \frac{d^2U(x_c)}{dx^2} = \frac{df_x}{dx} = -k, \tag{44}$$

while the critical position of the support is obtained from Eq. (22),

$$\frac{\partial E(R_c,x_c)}{\partial x} = \frac{dU(x_c)}{dx} - k(R_c - x_c) = 0. \tag{45}$$

The effective elastic constant between the tip and the cantilever, $\tilde{k}$ is extracted from the sawtooth graphs [for instance, Fig. 5(a)], and F_c can be then be obtained from Eq. (32) Finally, the numerical evaluation of the third derivative of $U(x)$ yields E_{eff} and Ω_{eff}. Then the coefficients in X and ΔF can be calculated.

We define

$$A \equiv \tilde{k}R_c\left(\frac{k_B}{E_{\text{eff}}}\right)^{2/3} \tag{46}$$

and

$$B \equiv \frac{2}{3}\frac{\Omega_{\text{eff}}^2}{2\pi\gamma}R_c\frac{k_B}{E_{\text{eff}}}, \tag{47}$$

and rewrite Eq. (31) as

$$F = F_c - AT^{2/3}\ln^{2/3}\left(B\frac{T}{v}\right), \tag{48}$$

which is proportional to the microscopic friction coefficient.

The numerical results obtained in this way for the various substrates are shown in Table III. This allows us to scale the data according to Eq. (31), with the result shown in Fig. 7. For these figures, we keep only temperatures and velocities that are clearly within the stick-slip regime. The collapse of all data shows clearly that Eq. (31) gives an adequate description of the stick-slip process even when local elasticity of the substrate is present. Note that the data points for the soft substrate ($\epsilon=0.1$) at 133 K and 5 and 10 nm/sec do not

TABLE III. Numerical values of the parameters obtained from the scaling analysis of Fig. 7.

	F_c (nN)	A (10^{-3} nN/K$^{2/3}$)	B (m/sec K)
0.01	0.57	2.0	30.4
0.05	0.26	1.5	14.9
0.1	0.045	0.79	4.3

scale well with the rest of the data. This is because soft substrates require a considerably smaller normal load than harder substrates. The small normal load leads to a small effective potential barrier. Starting from high temperatures where k_BT is comparable to the effective potential barrier, the tip is no longer confined to the potential minimum. So for temperatures higher than 93 K the transition is not confined to the small regime around the critical position, which means Eq. (31) does not apply.

We also studied the distribution of force maxima from Eq. (28), under the assumption $F_m=\tilde{k}R_m$. For hard ($\epsilon=0.1$ strain) substrate at 293 K, we calculated the force maxima distribution for velocities $v_1=25$ nm/sec and $v_2=1$ μm/sec. For these choices, $X(v_1)=3.6\times10^2$ and $X(v_2)=8.9$. Other parameters obtained from the numerical simulations and used in the theoretical calculations are $E_{\text{eff}}=0.6$ eV and $R_c=0.86$ nm. The comparison of theoretical and numerical results is shown in Fig. 8. The theoretical and numerical results agree very well at low velocities although deviations are seen at larger velocities (1 μm/sec). These deviations are because linear friction ($F=M\gamma v$) becomes comparable to the stick-slip friction [F given by Eq. (31)] at large velocity.

IV. CONCLUSIONS

In this paper, we studied the dependence of the friction coefficient μ on the surface roughness. We pointed out the importance of using the mass density and explained previous numerical results concerning the dependence of forces on the real area of contact for rough surfaces. As well, we have made a prediction of a weak anomaly in the friction coefficient, which is dependent on the apparent area of the rough surface. We also developed a method to calculate the atomic friction based on thermally activated stochastic processes. A numerical model was set up to test our analytical results. The results in this paper and our previous work [39] show that this nonlinearly logarithmic dependence on scanning velocity and temperature is universal. It does not depend on the particular form of surface potential in the model nor on the substrate's elastic properties, and should be experimentally observable on different substrates. In order to study thermal effects, we used a Langevin equation to describe the thermally activated motion of the FFM tip. This method allowed us to simulate time scales ranging from a few seconds to a few minutes, which match the experiment time scales. Finally, the simplified Tomlinson model we used in this paper is very successful in probing problems related to stick-slip motion in the lateral direction and can also be used to study the relationship between the friction and normal load [9], allowing one to calculate the effective microscopic friction coefficient $\mu_{\text{micro}}\propto F$. To test those results experimentally, it would be particularly valuable to consider an extended range of temperatures and velocities, obtaining not only the dependence of the friction force on those quantities, but the distribution function of such forces as well. The parameters extracted from such comparisons provide direct, feasible, and simple access to the fundamental description of friction at the atomic scale.

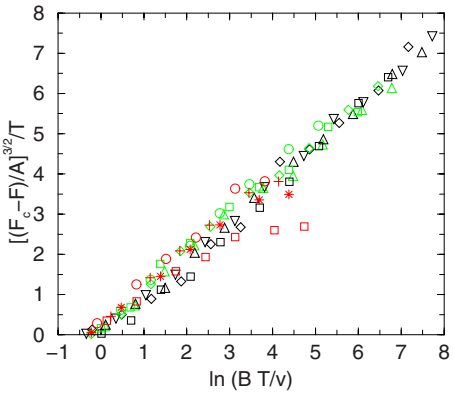

FIG. 7. (Color online) Scaling for the data of three different substrates. Black, green, and red symbols correspond to hard ($\epsilon=0.01$), mid-soft ($\epsilon=0.05$), and soft ($\epsilon=0.1$) substrates respectively.

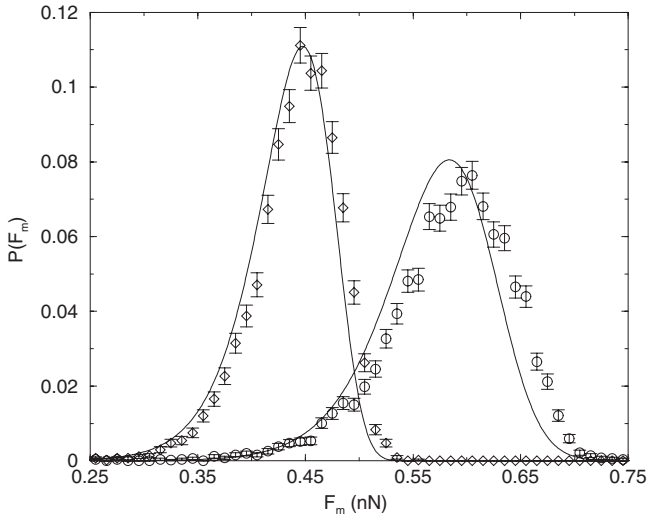

FIG. 8. Normalized distribution, with statistical error bar, of the maxima of the friction force F_m for hard ($\epsilon=0.01$) substrate at 293 K with $v=2$ (diamonds) and 1 μm/sec (circles). Solid lines are theoretical results.

ACKNOWLEDGMENTS

We thank Peter Grütter, Roland Bennewitz, François Drolet, and Lyne Cormier for interesting discussions. This work was supported by the Natural Sciences and Engineering Research

Council of Canada, the Canada Research Foundation on Value-Added Paper, and le Fonds Québécois de la Recherche sur la Nature et les Technologies.

APPENDIX

In this appendix, we show how Eqs. (24) and (25), leading to Eq. (1), can be understood in terms of a generic potential $E(R,x)$. We only assume that the potential consists of a metastable minimum and that R is a parameter that controls the height of the potential barrier. At $R=0$, the local minimum and maximum of the potential are denoted by $x_{\pm}^{0}$ obtained from the solution of

$$\left.\frac{\partial E(0,x)}{\partial x}\right|_{x_{\pm}^{0}} = 0. \tag{A1}$$

The barrier height for thermal activation is then $\Delta E_0 = E(0,x_+) - E(0,x_-)$. For nonzero but small values of R, the barrier height can be found from a simple Taylor expansion around $R=0$ and $x_{\pm}^{0}$.

$$\Delta E(R) = \Delta E(0) + R\left(\frac{\partial E(0,x_+^0)}{\partial R} - \frac{\partial E(0,x_-^0)}{\partial R}\right) \tag{A2}$$

is linear in the control parameter R. However, this expansion is valid only if the second term in Eq. (A2) is much smaller than the unperturbed barrier height ΔE_0. As a renormalization group analysis clearly shows [33], this "linear response" is not valid in the cases where the thermally activated behavior takes place when the barrier is extremely small.

Instead, the expansion of the potential must be made with respect to the point where $\Delta E=0$. A vanishing energy barrier corresponds to an inflection point of the potential $E(R,x)$; this point is located at the position x_c, given by Eqs. (21) and (22). The spinodal point of the potential, R_c, corresponds to the of the control parameter for which $\Delta E(R_c)=0$. Denoting $f=1-R/R_c$, we look for the new minimum and maximum by Taylor expansion in the proximity of R_c and x_c:

$$\begin{aligned} 0 &= \frac{\partial}{\partial x}E(R_c(1-f),x_c \pm \delta x) \\ &= \frac{\partial E(R_c,x_c)}{\partial x} - fR_c\frac{\partial^2 E(R_c,x_c)}{\partial R\,\partial x} \\ &\quad \pm \delta x\frac{\partial^2 E(R_c,x_c)}{\partial x^2} + \frac{1}{2}\delta x^2\frac{\partial^3 E(R_c,x_c)}{\partial x^3} + \cdots \end{aligned} \tag{A3}$$

where $\delta x = x - x_c$. The first term of the expansion as well as the term of order $O(\delta x)$ vanish from the definition of the spinodal point and terms of higher order than $O(R_c f)$ can be omitted from the calculation. The displacement $\delta x \sim O(f^{1/2})$, or more precisely

$$\delta x^2 = 2fR_c\left(\frac{\partial^2 E(R_c,x_c)}{\partial R\,\partial x}\right)\left(\frac{\partial^3 E(R_c,x_c)}{\partial x^3}\right)^{-1}, \tag{A4}$$

or, in the specific case of a potential of the form Eq. (18),

$$\delta x^2 = 2fR_c\left(\frac{\partial^2 K(R_c,x_c)}{\partial R\ \partial x}\right)\left(\frac{\partial^3 U(x_c)}{\partial x^3}\right)^{-1}. \tag{A5}$$

The barrier height is thus

$$\begin{aligned} \Delta E(f) &= E(R_c(1-f),x_c+\delta x) - E(R_c(1-f),x_c-\delta x) \\ &\simeq -2fR_c\delta x\frac{\partial^2 E(R_c,x_c)}{\partial R\ \partial x} + \frac{1}{3}\delta x^3\frac{\partial^3 E(R_c,x_c)}{\partial x^3} \equiv E_{\mathrm{eff}}f^{3/2}. \end{aligned} \tag{A6}$$

Again specializing to the case of Eqs. (18) and (35)

$$E_{\mathrm{eff}} = \frac{4\sqrt{2}}{3}k^{3/2}R_c^{3/2}\left(\frac{\partial^3 U(x_c)}{\partial x^3}\right)^{-1/2}. \tag{A7}$$

The oscillation frequency in the local minimum and in the "inverted" potential are also needed for a complete determination of the Kramers rate [49]. Up to $O(f^{1/4})$, the oscillation frequency of the potential, $\Omega(f,x_c+\delta x)=\Omega(f,x_c-\delta f)=\Omega(f)$, with

$$\Omega^2 = \frac{1}{M}\frac{\partial^2 E(R_c(1-f),x_c-\delta x)}{\partial x^2} \tag{A8}$$

$$= \frac{1}{M}\left(\frac{\partial^2 E(R_c,x_c)}{\partial x^2} - fR_c\frac{\partial^3 E(R_c,x_c)}{\partial R\,\partial x^2} - \delta x\frac{\partial^3 E(R_c,x_c)}{\partial x^3} + \cdots\right). \tag{A9}$$

However, since $\delta x \sim O(f^{1/2})$, to lowest order,

$$\Omega^2 \simeq -\frac{\delta x}{M}\frac{\partial^3 E(R_c,x_c)}{\partial x^3} \tag{A10}$$

and $\Omega \equiv \Omega_{\mathrm{eff}} f^{1/4}$, where

$$\Omega_{\mathrm{eff}}^2 = -\frac{1}{M}(2k)^{1/2}R_c^{1/2}\left(\frac{\partial^3 U(x_c)}{\partial x^3}\right)^{1/2}. \tag{A11}$$

[1] E. Meyer, R. M. Overney, K. Dransfeld, and T. Gyalog, *Nanoscience: Friction and Rheology on the Nanometer Scale* (World Scientific, Singapore, 1998).

[2] F. Heslot, T. Baumberger, B. Perrin, B. Caroli, and C. Caroli, Phys. Rev. E **49**, 4973 (1994); C. Caroli and B. Velicki, J. Phys. I **7**, 1391 (1997).

[3] J. A. Greenwood and J. B. P. Williamson, Proc. R. Soc. London, Ser. A **295**, 300 (1966). They find that the behavior of the normal load as a function of the contact area is almost constant. They nevertheless do find some power-law-like behavior (with effective exponent of 0.9) in the electrical resistivity. We expect the latter is not an asymptotic power law, but rather a slow crossover to linear behavior.

[4] B. J. Persson, *Sliding Friction* (Springer, Berlin, 1998).

[5] *Handbook of Micro/Nanotribology*, edited by B. Bhushan (CRC Press, Boca Raton, FL, 1999).

[6] B. N. J. Persson, O. Albohr, F. Mancosu, V. Peveri, V. N. Samoilov, and I. M. Sivebaek, Wear **254**, 835 (2003).
[7] C. M. Mate, G. M. McClelland, R. Erlandsson, and S. Chiang, Phys. Rev. Lett. **59**, 1942 (1987).
[8] E. Gnecco, R. Bennewitz, T. Gyalog, Ch. Loppacher, M. Bammerlin, E. Meyer, and H.-J. Guntherodt, Phys. Rev. Lett. **84**, 1172 (2000).
[9] E. Riedo, E. Gnecco, R. Bennewitz, E. Meyer, and H. Brune, Phys. Rev. Lett. **91**, 084502 (2003).
[10] S. Maier, Y. Sang, T. Filleter, M. Grant, R. Bennewitz, E. Gnecco, and E. Meyer, Phys. Rev. B **72**, 245418 (2005).
[11] A. Schirmeisen, D. Weiner, and H. Fuchs, Phys. Rev. Lett. **97**, 136101 (2006).
[12] M. Evstigneev, A. Schirmeisen, L. Jansen, H. Fuchs, and P. Reimann, Phys. Rev. Lett. **97**, 240601 (2006).
[13] B. Luan and M. O. Robbins, Phys. Rev. E **74**, 026111 (2006).
[14] S. Roux, J. Schmittbuhl, J. P. Vilotte, and A. Hansen, Europhys. Lett. **23**, 277 (1993).
[15] B. N. J. Persson, J. Chem. Phys. **115**, 3840 (2001).
[16] B. N. J. Persson, Phys. Rev. Lett. **87**, 116101 (2001).
[17] G. G. Batrouni, A. Hansen, and J. Schmittbuhl, Europhys. Lett. **60**, 724 (2002).
[18] S. Hyun, L. Pei, J.-F. Molinari, and M. O. Robbins, Phys. Rev. E **70**, 026117 (2004).
[19] S. Hyun and M. O. Robbins, Tribol. Int. **40**, 1413 (2007).
[20] C. Campana, Phys. Rev. B **75**, 155419 (2007).
[21] C. Campana and M. H. Muser, Europhys. Lett. **77**, 38005 (2007).
[22] J. A. Greenwood and J. J. Wu, Meccanica **36**, 617 (2001).
[23] S. Ganti and B. Bhushan, Wear **180**, 17 (1995).
[24] A. Majumdar and B. Bhushan, J. Tribol.. **113**, 1 (1991).
[25] P. J. Mangin, M. C. Béland, and L. M. Cormier, in *Products of Papermaking*, edited by C. F. Barker, Transactions of the 10th Fundamental Research Symposium, Oxford, England (Pira International, Leatherhead, 1993), p. 1397.
[26] F. Drolet and T. Uesaka, in *Advances in Paper Science and Technology*, edited by J. L'Anson, Transactions of the 13th Fundamental Research Symposium (Bury, United Kingdom, 2005), Vol. 2, p. 1139–1154.
[27] S. Morita, S. Fujisawa, and Y. Sugawara, Surf. Sci. Rep. **23**, 1 (1996).
[28] T. Bouhacina, J. P. Aime, S. Gauthier, D. Michel, and V. Heroguez, Phys. Rev. B **56**, 7694 (1997).
[29] G. A. Tomlinson, Philos. Mag. **7**, 905 (1929).
[30] D. Tomanek *et al.*, Europhys. Lett. **15**, 887 (1991); T. Gyalog *et al.*, *ibid.* **31**, 269 (1995); T. Gyalog and H. Thomas, Z. Phys. B: Condens. Matter **104**, 669 (1997).
[31] H. Hölscher, U. D. Schwarz, and R. Wiesendanger, Europhys. Lett. **36**, 19 (1996); Surf. Sci. **375**, 395 (1997); O. Zwörner *et al.*, Appl. Phys. A: Mater. Sci. Process. **66**, S263 (1998).
[32] M. H. Muser, Phys. Rev. Lett. **89**, 224301 (2002).
[33] J. D. Gunton and M. C. Yalabik, Phys. Rev. B **18**, 6199 (1978).
[34] C. Unger and W. Klein, Phys. Rev. B **29**, 2698 (1984).
[35] J. Kurkijarvi, Phys. Rev. B **6**, 832 (1972).
[36] L. D. Jackel, W. W. Webb, J. E. Lukens, and S. S. Lei, Phys. Rev. B **9**, 115 (1974).
[37] A. Garg, Phys. Rev. B **51**, 15592 (1995).
[38] D. S. Fisher, Phys. Rev. B **31**, 1396 (1985).
[39] Y. Sang, M. Dube, and M. Grant, Phys. Rev. Lett. **87**, 174301 (2001).
[40] O. K. Dudko, A. E. Filippov, J. Kalfter, and M. Urbakh, Chem. Phys. Lett. **352**, 499 (2002).
[41] A. L. Barab'asi and H. E. Stanley, *Fractal Concepts in Surface Growth* (Cambridge University Press, Cambridge, U.K., 1995).
[42] The length l_δ can be obtained from a microscopic model of roughness; see e.g., J. Krug, Adv. Phys. **46**, 139 (1997).
[43] L. D. Landau and E. M. Lifshitz, *Theory of Elasticity* (Pergamon, Oxford, 1970).
[44] R. Kant, Phys. Rev. E **53**, 5749 (1996).
[45] H. J. Hertz, J. Reine Angew. Math. **92**, 156 (1881).
[46] K. L. Johnson, *Contact Mechanics* (Cambridge University Press, Cambridge, U.K., 1985).
[47] In principle, the combined product of density and curvature should be averaged over the fluctuations of the surface: $\langle \nabla^2 h \theta(z-h) \rangle$. A separate average is appropriate since each quantity depends on different regions of the frequency of fluctuations. The curvature is dominated by the large-wavelength part of the spectrum while the density is dominated by the low-wavelength components. Again, it is straightforward to show this for a Gaussian interface.
[48] The neglect of the y coordinate has no influence on the results presented in this paper.
[49] P. Hanggi, P. Talkner, and M. Borkocev, Rev. Mod. Phys. **62**, 251 (1990).
[50] A. Buldum and S. Ciraci, Phys. Rev. B **55**, 2606 (1997).
[51] Note that, at very low velocities, thermally activated events can occur before the spinodal limit considered here. However, this corresponds to velocities below 1 nm/sec, well below the experimental range [39].
[52] M. P. Allen and D. J. Tildesley, *Computer Simulations of Liquids* (Clarendon, Oxford, 1990).
[53] D. Forster, *Hydrodynamic Fluctuations, Broken Symmetry and Correlation Functions* (Addison-Wesley, Reading, MA, 1983).
[54] A detailed analysis shows that the dissipation coefficient γ may itself depend on the position of the atoms. This effect is neglected here. See, e.g., L. N. Kantorovich, Phys. Rev. B **64**, 245409 (2001).
[55] P. M. Chaikin and T. C. Lubensky, *Principles of Condensed Matter Physics* (Cambridge University Press, Cambridge, U.K., 1995).